

# Effect of Ageing of Gas Diffusion Layers on the Water Distribution in Flow Field Channels of Polymer Electrolyte Membrane Fuel Cells

Juliane Kätzel <sup>a</sup>, Henning Markötter <sup>a,b</sup>, Tobias Arlt <sup>a</sup>, Merle Klages <sup>c</sup>, Jan Haussmann <sup>c</sup>, Matthias Messerschmidt <sup>c</sup>, Nikolay Kardjilov<sup>a</sup>, Joachim Scholta <sup>c</sup>, John Banhart <sup>a,b</sup>, Ingo Manke <sup>a</sup>

a) Helmholtz-Zentrum Berlin (HZB), Hahn-Meitner-Platz 1, 14109 Berlin, Germany

b) Technische Universität Berlin (TUB), Straße des 17. Juni 135, 10623 Berlin, Germany

c) Zentrum für Sonnenenergie- und Wasserstoff-Forschung Baden Württemberg (ZSW), Helmholtzstraße 8, 89081 Ulm, Germany

## Keywords

Polymer electrolyte membrane fuel cell, gas diffusion layer, artificial ageing, neutron radiography, water distribution, droplet size distribution

## Abstract

We present a quantitative analysis of the influence of artificial ageing of gas diffusion layers (GDL) on the water distribution and transport in polymer electrolyte membrane fuel cells (PEMFCs) during cell operation. Water droplet size distributions are measured by means of in-operando neutron radiography. We find a strong correlation between droplet size distribution and GDL ageing time: With increasing GDL ageing, water droplet sizes in the flow field channels strongly decrease, indicating an ineffective water transport that leads to a reduced cell performance. This effect can be assigned to water accumulations on the GDL surface that block the gas supply towards the catalyst layer.

## 1. Introduction

Fuel cells will play an important role in a future hydrogen economy [1-3]. Because of their high power density and flexible operating range, low-temperature polymer electrolyte membrane fuel cells (PEMFC) are suitable for mobile applications, e.g. in vehicles [4] or to provide combined heat and power in stationary energy systems [5, 6]. A decisive factor for the optimal operation of PEMFCs is a balanced water management [7, 8].

On the one hand, the membrane of the PEMFC must be sufficiently humidified to be proton conductive, but on the other hand, it must not accumulate too much water since otherwise the pores of the gas diffusion layer (GDL) will be clogged and the supply of the catalyst layer with reactant gases obstructed [3, 7, 9-12]. During long-term operation, the properties of the GDL fibres change

[13, 14]. Many published works examine the water transport and distribution with synchrotron X-ray imaging, which is characterised by a high temporal and spatial resolution [9-11]. Others have visualised the water transport with transparent cell materials [15]. In this article, the effect of GDL ageing on the water balance of a fuel cell is shown by neutron imaging [16-21]. The strong attenuation of the neutron beam by hydrogen combined with the high transmission through the fuel cell components allows for a high contrast and a quantitative investigation of the water distribution [22-26].

## **2. Experimental**

### **2.1. Neutron radiography**

The imaging instrument CONRAD (**CO**ld **N**eutron **R**adiography) is designed for materials and structure research [27]. It provides the possibility of creating radiographs using cold neutrons. The neutron beam at CONRAD is formed by a neutron guide and is polychromatic with wavelengths between 2 to 6 Å and a maximum intensity at about 3.0 Å. The measurements of the fuel cells discussed here are performed 10 m behind the exit of the neutron guide. Although this large distance leads to a lower neutron flux density and thus a lower image repetition frequency, i.e. a loss of temporal resolution, it allows for a higher spatial resolution [28].

Behind the sample, a detector system consisting of a scintillator, mirror, lens and CCD camera is placed [28-30]. When the neutrons, which are transmitted and scattered by the sample, hit the scintillator, photons in the visible spectrum are emitted. The scintillator used for the measurements is a lithium fluoride crystal with silver-doped zinc sulfide (6 LiF / ZnS (Ag)).

The photons are projected onto the camera by a mirror/lens combination. The Andor DW436 camera used contains a 16 bit chip with (2048 x 2048) pixels, each of a size of 13.5 µm [27]. The CCD sensor is continuously cooled to below -50° C to keep thermal noise as low as possible. With the optics used an imaging field of view of (108 x 108) mm<sup>2</sup> with a pixel size of 53 µm is achieved. Each radiographic projection is acquired with an exposure time of 16 s.

### **2.2. Fuel cell setup**

Four single cells with an active area of 10 cm x 10 cm are investigated. For each cell, a differently aged GDL is used (see details below). A GORE® PRIMEA 5761™ catalyst coated membrane is applied. The regulation of the cell temperature is carried out by using a cooling circuit with deuterium oxide (D<sub>2</sub>O). Compared to hydrogen, the attenuation coefficient of deuterium is much smaller [31, 32]. As a result, D<sub>2</sub>O hardly attenuates a neutron beam and can only be seen faintly in radiographs. The flow field of the cooling circuit is embedded in the backside of the bipolar plates and is connected with a secondary water coolant circuit via a heat exchanger. Into the graphite material of the bipolar plates, three ~0.8 mm wide meander-shaped channels are milled, in which the supply gases, hydrogen on the anode and air on the cathode side, flow from top to bottom. Figure 1 shows the cell and the flow field of the cathode side. Note that the anode and cathode flow fields are identical, but start in opposite corners, which means that in the radiographs the curves of the anode channels overlap with the ribs at the cathode side and vice versa. The presented measurements are conducted at a current density of 1 A cm<sup>-2</sup> and a cell temperature of 50°C, while the cell is supplied with gases of 100% relative humidity. Via gas flow controllers the ratio of the supplied and consumed gases is set to four for the anode (H<sub>2</sub>) as well as the cathode (air) side.

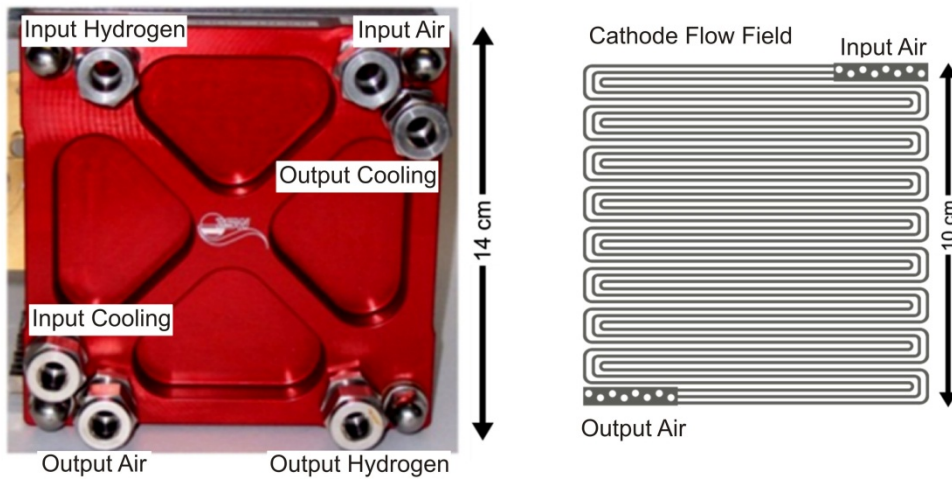


**Figure 1: PEMFC with an active area of 100 cm<sup>2</sup> used for neutron radiography (left) and the flow field of the cathode side with three meander-shaped channels (right).**

To simulate the effect of chemical ageing on cell performance the GDLs of type Sigracet® SGL 25BC are subjected to accelerated ageing at the ZSW.

### 2.3. Accelerated ageing process

Degradation effects of fuel cells can usually only be registered after several hundred hours of continuous operation. Therefore, accelerated ageing methods are used to enable their characterization in reasonable times. Using ex-situ ageing ensures that the desired ageing process is isolated from other degradation mechanisms in the fuel cell. The method used here for accelerated ex-situ ageing of the GDL material is conducted with hydrogen peroxide (H<sub>2</sub>O<sub>2</sub>). The gas diffusion layers are exposed to a solution of 30% H<sub>2</sub>O<sub>2</sub> (diluted with water) at 90°C for several hours. After this, the GDL is washed for one hour in distilled water to remove the H<sub>2</sub>O<sub>2</sub> residues and then dried at 80°C. For our study, GDLs of type SGL 25BC were chosen. Both the cathodic and the anodic GDLs of the four test cells were subjected to accelerated ageing by H<sub>2</sub>O<sub>2</sub> treatment of the GDLs for 0 h, 4 h, 8 h and 24 h.

### 2.4. Analysis of water droplets in the channel

As one main purpose of this work is the analysis of water droplets in the channel system the procedures to characterize them are described in this chapter. The thickness of the water layer through which the beam locally passes is calculated by Lambert-Beer's law [31, 33, 34]. By setting a grey value as a threshold, individual water accumulations above a certain thickness are extracted and size and number of them are determined (The effect of different parameters is shown in Figure 2). The threshold for this droplet selection must be chosen appropriately. If it is set too large, a high proportion of the water accumulation shown in the radiographs no longer appears in the resulting images (blue arrows in Figure 2 A). If the selected threshold is too low it will not be possible to distinguish single water droplets from one another (see red arrows). As a good compromise, a threshold value of 200 μm has been used for the radiographs shown here. This threshold is also sufficiently high to make GDL water accumulations under the ribs invisible.

The number and size of water accumulations in the channels are determined with the "Analyze Particle" function implemented in the open-source image processing software ImageJ. Artefacts arising due to image noise are removed by setting a minimum lateral size for the selection of water

agglomerations. The value for this second criterion is set to 10 pixels (equivalent to 0.028 mm<sup>2</sup>). The effect of different settings can be seen in Figure 2B.

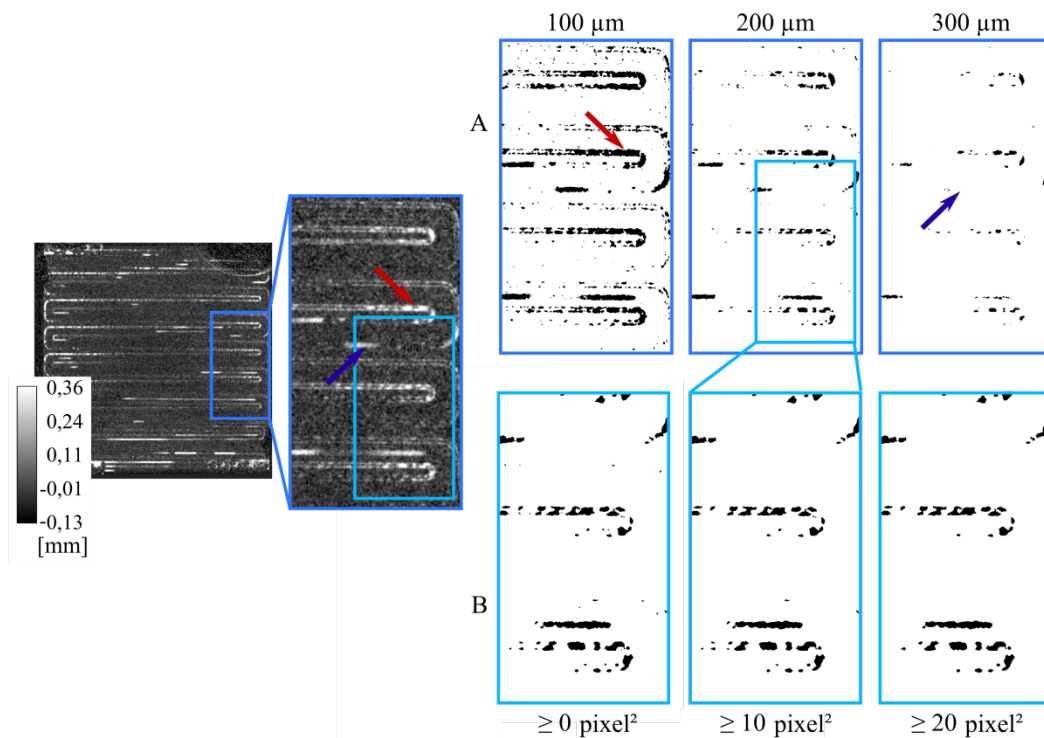


**Figure 2: Determination of suitable radiogram analysis parameters illustrated using a sample radiogram (left, given for the complete cell and a magnified cut out). Right: Cut out of detected droplets using (A) three different values for the threshold of the water thickness and (B) three different values for the minimum droplet size with the threshold being 200 μm. Both criteria have to be satisfied.**

According to the specified minimum thickness and minimum size in pixels, the minimum volume of the selected water droplets for being detected is ~5 nl. Not all the water in the channel fits in these criteria. At the same time also water agglomerations could be selected, which are incidentally overlapping in the projection and reach a thickness of more than 200 μm. However, the method is suitable for qualitative studies of droplet size distributions and the transport behaviour from the GDL into the channel and the comparison of aged and non-aged materials.

### 3. Results

Ex-situ investigations revealed a decrease in contact angle of water and carbon fibres due to ageing in H<sub>2</sub>O<sub>2</sub> solution, which corresponds to a decrease in hydrophobicity [35]. The contact angle of water droplets on the GDL surface decreases from 160° (0 h) to about 98° (24 h H<sub>2</sub>O<sub>2</sub> ageing). Correspondingly, the voltage of the test cells decreases. At 1 A cm<sup>-2</sup> current density, the voltage obtained drops from 650 mV (0 h) to 350 mV (24 h). Although the water production rate is equal for all four cells, the way the water is moved out of the cell is observed to vary with the duration of ageing.

The volume of each selected droplet is calculated via the lateral size and average thickness. A result of the cell containing the pristine material at a current density of 1 A cm<sup>-2</sup> is shown exemplarily in Figure 3. For each radiogram, the number (upper) and the average volume (lower) of the water droplets in the three flow field channels are determined individually. In Figure 4, the water

accumulations are presented for each channel in an individual colour code within a time interval marked with a vertical grey bar in the diagrams of Figure 3.

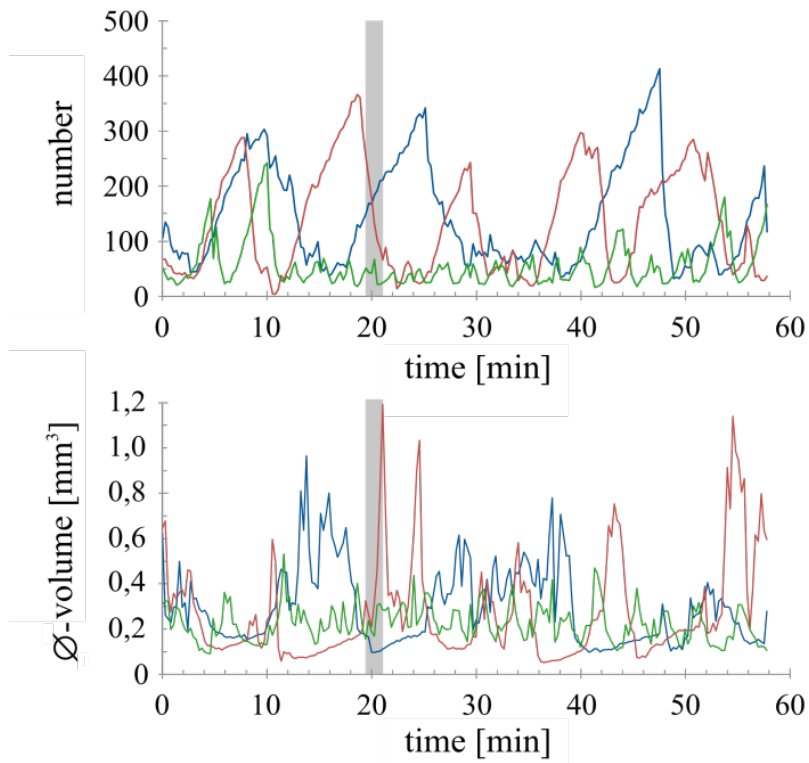


**Figure 3: Number and average volume of water droplets of the cell containing pristine GDL material as a function of operation time. Cell operated at 100% relative gas humidity and a current density of 1 A/cm<sup>2</sup>. Data determined by image analysis of sequences of radiographs. Each curve corresponds to one of the three flow field channels. Vertical grey bar: see Figure 4.**

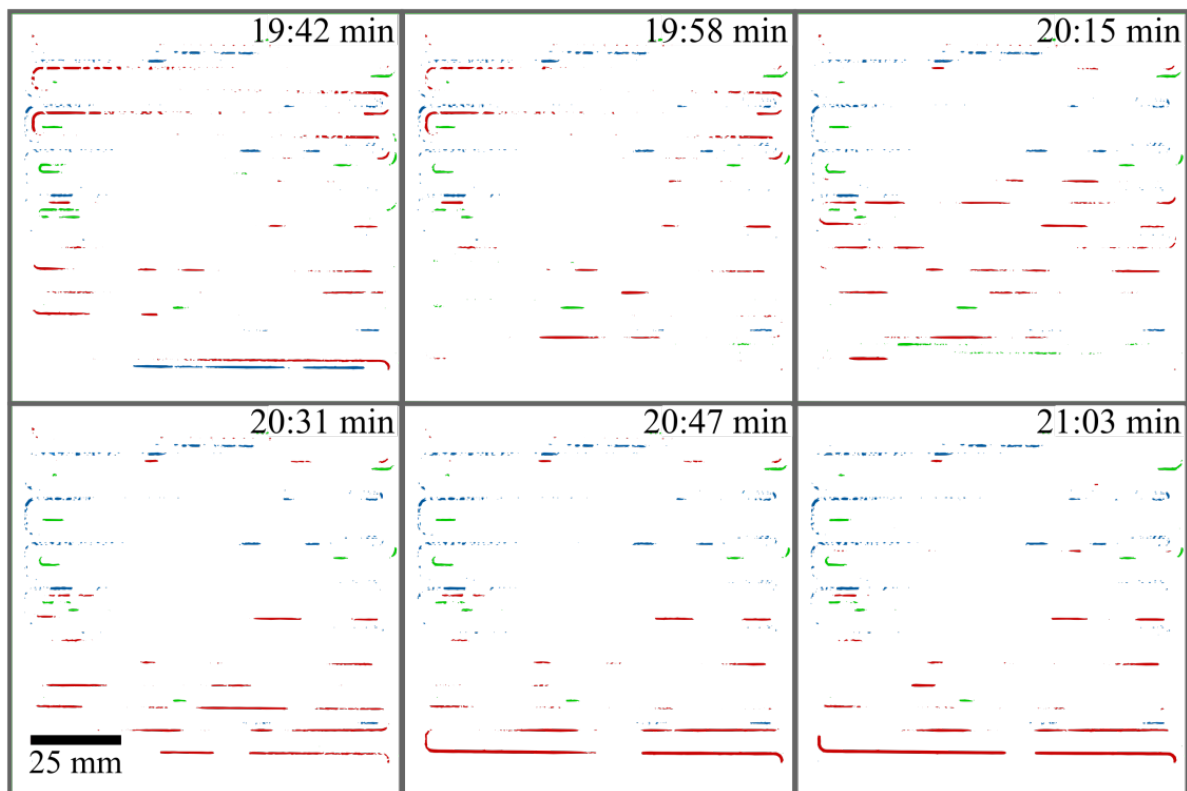


**Figure 4: Image series of the water agglomerations in the cell with pristine material at 100% relative gas humidity at 1 A/cm<sup>2</sup> taken at the time marked by a vertical bar in Figure 3. Each colour corresponds to one of the three flow field channels.**

Each of the individually coloured graphs represents one channel of the three-fold meander. The number and average volume of the water droplets vary in the different channels. The average drop volume and the number of droplets show a time delayed correlation since the average drop volume peaks when the number of droplets is decreasing. This confirms that the water droplets are combined to bigger water agglomerations when they are removed through the channel system.

For determining the size distribution of the water droplets they are grouped into classes according to their volume. Figure 5 shows results for differently aged GDLs. The complete image series of about 60 min is taken into account, i.e. the distribution is averaged this period. The equivalent diameter of a sphere of the same volume is plotted on the ordinate axis. The division of the classes takes place in 100  $\mu\text{m}$  increments. Due to the high number of small water droplets their share of the total water amount is not negligible despite a smaller individual volume. Note that only water droplets with an equivalent diameter of more than 200  $\mu\text{m}$  ( $\sim 5 \text{ nl}$ ) are taken into account, based on the two predetermined criteria (see Figure 2). The curve is slightly distorted to lower numbers in the region of small agglomerations, because some droplets with volumes exceeding 5 nl are not selected, when only one of the two criteria is satisfied. For example, thin films on the channel walls that are below the specified threshold criterion of 200  $\mu\text{m}$  thickness are not considered even though their total volume is larger than 5 nl. In the diagrams of cells with non-aged and 4 hours aged GDL, water accumulations are listed that have a calculated equivalent diameter of more than 3.6 mm. These are mostly elongated water accumulation in the channel, as can be seen at the bottom of the corresponding radiographs in Figure 4. The median of the droplet size distribution is indicated by a vertical bar that divides the diagram into two parts, whereby 50% of the water volume appears in smaller and 50% in larger droplets. With increased ageing of the GDL, the median value changes to

smaller droplet diameters. This means that smaller water agglomerations form with increased GDL ageing.

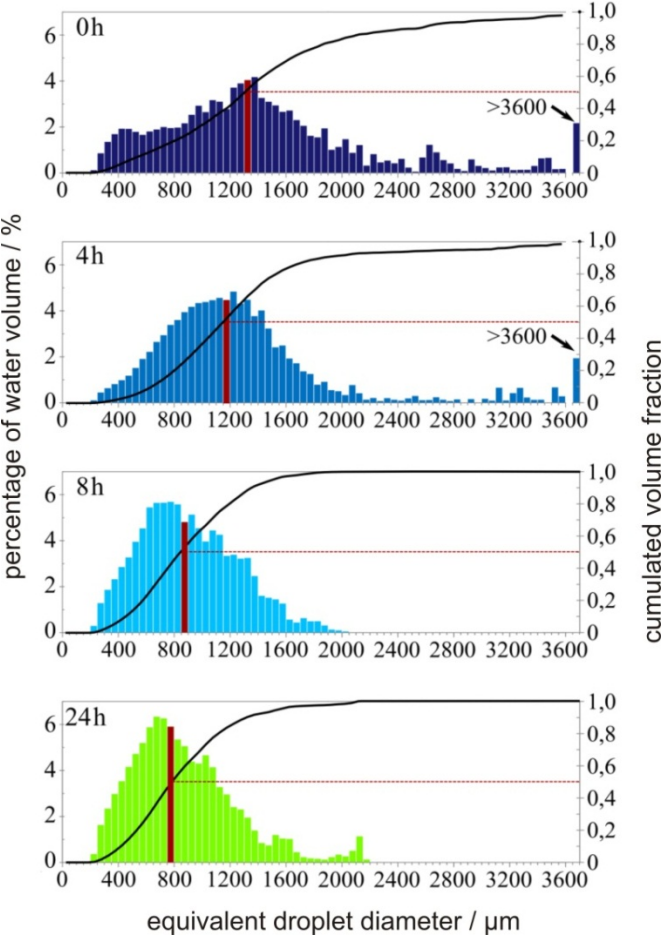


Figure 5: Droplet size distribution (histogram) and cumulated volume fraction (black line) of water in the flow field of the cells artificially aged for 0 h, 4 h, 8 h and 24 h. The median of the distribution is marked in red.

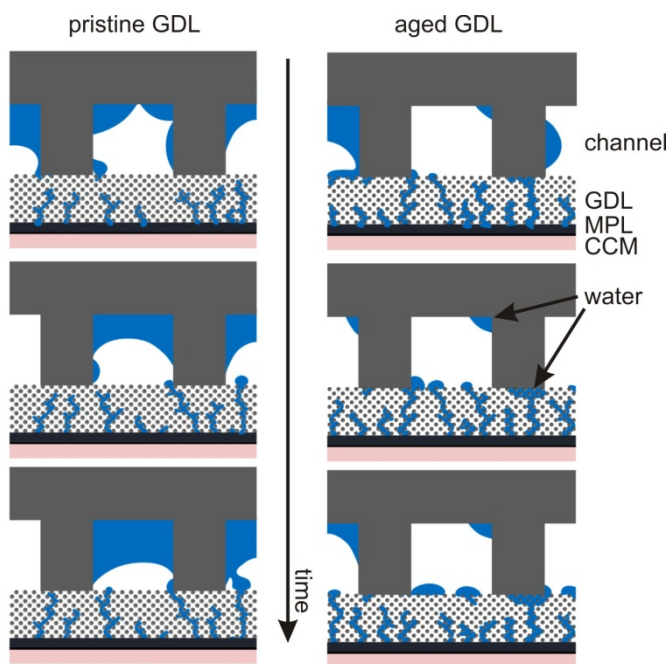


Figure 6: Schematic illustration of possible water formation in a cell containing a new (left) or aged (right) GDL. After some time of operation, water droplets accumulate preferably at the surface of the aged GDL. Liquid water is rendered in blue.

#### 4. Discussion

Artificial ageing is only conducted with the GDLs, while the rest of the cells remains the same in all the experiments. This allows us to conclude that in the cell containing an aged GDL, water droplets accumulate rather on the GDL surface instead of on the channel walls as a result of the lower hydrophobicity of the GDL. In contrast, in the cell containing pristine GDL material the droplets in the channel are found to agglomerate preferably at the outer wall, which has previously also been reported by Markötter et al. and Krüger et al. [36, 37]. Water transport from the GDL into the channel for both the pristine and aged materials is sketched schematically in Figure 6. Accordingly, the water agglomerations on the aged GDL surface lead to a modified water transport in the flow field and also block the path of the supply gases towards the catalyst layer. This results in a less efficient water and gas transport. Therefore, the decrease in water droplet size in the channels with increasing GDL ageing directly and indirectly affects the obtained cell voltage.

#### 5. Conclusions and outlook

We investigate the influence of artificial ageing of GDL materials on the water transport in a PEMFC in-operando with neutron radiography. Fewer large water agglomerations form in the channel with increased ageing of the GDL material and the average size of the water agglomerations decreases. This effect can be explained by water droplets on the GDL surface that change the overall water and gas distribution in the channels. These findings give new insights into the general relationship between GDL ageing and fuel cell performance and provide hints for further optimization of the materials to counteract the negative effect of ageing on the water transport. Fuel cell materials aged under real conditions inside a fuel cell stack should be investigated in future in order to validate and optimise the artificial ageing procedures.

## Acknowledgement

This project was funded by the German Federal Ministry of Economics and Technology (grant 03ET2007).

## References

- [1] G. Hoogers, CRC Press LLC, Boca Raton, FL, 2003.
- [2] W. Vielstich, A. Lamm, H.A. Gasteiger, John Wiley & Sons, Chichester, 2003.
- [3] C. Hartnig, C. Roth, Preface, in: C. Hartnig, C. Roth (Eds.) *Polymer Electrolyte Membrane and Direct Methanol Fuel Cell Technology*, Woodhead Publishing, 2012, pp. xvii-xviii.
- [4] V. Mehta, J.S. Cooper, *J Power Sources*, 114 (2003) 32-53.
- [5] L. Barelli, G. Bidini, F. Gallorini, A. Ottaviano, *Applied Energy*, 91 (2012) 13-28.
- [6] G. Gigliucci, L. Petrucci, E. Cerelli, A. Garzisi, A. La Mendola, *J Power Sources*, 131 (2004) 62-68.
- [7] C.-Y. Wang, Two-phase flow and transport, in: W. Vielstich, A. Lamm, H.A. Gasteiger (Eds.) *Handbook of Fuel Cells – Fundamentals, Technology and Applications*, John Wiley & Sons, Chichester, 2003, pp. 337–347.
- [8] C.-Y. Wang, *Chem Rev*, 104 (2004) 4727-4766.
- [9] H. Markötter, R. Alink, J. Haußmann, K. Dittmann, T. Arlt, F. Wieder, C. Tötze, M. Klages, C. Reiter, H. Riesemeier, J. Scholta, D. Gerteisen, J. Banhart, I. Manke, *International Journal of Hydrogen Energy*, 37 (2012) 7757-7761.
- [10] J. Haußmann, H. Markötter, R. Alink, A. Bauder, K. Dittmann, I. Manke, J. Scholta, *J Power Sources*, 239 (2013) 611-622.
- [11] R. Alink, J. Haußmann, H. Markötter, M. Schwager, I. Manke, D. Gerteisen, *J Power Sources*, 233 (2013) 358-368.
- [12] J.P. Owejan, T.A. Trabold, D.L. Jacobson, M. Arif, S.G. Kandlikar, *International Journal of Hydrogen Energy*, 32 (2007) 4489-4502.
- [13] T. Arlt, I. Manke, K. Wippermann, C. Totzke, H. Markotter, H. Riesemeier, J. Mergel, J. Banhart, *Electrochem Commun*, 13 (2011) 826-829.
- [14] T. Arlt, I. Manke, K. Wippermann, H. Riesemeier, J. Mergel, J. Banhart, *J Power Sources*, 221 (2013) 210-216.
- [15] A. Bozorgnezhad, M. Shams, H. Kanani, M. Hasheminasab, G. Ahmadi, *International Journal of Hydrogen Energy*, 40 (2015) 2808-2832.
- [16] R.J. Bellows, M.Y. Lin, M. Arif, A.K. Thompson, D. Jacobson, *J Electrochem Soc*, 146 (1999) 1099-1103.
- [17] C. Hartnig, I. Manke, N. Kardjilov, A. Hilger, M. Grünerbel, J. Kaczerowski, J. Banhart, W. Lehnert, *J Power Sources*, 176 (2008) 452-459.
- [18] H. Markötter, I. Manke, R. Kuhn, T. Arlt, N. Kardjilov, M.P. Hentschel, A. Kupsch, A. Lange, C. Hartnig, J. Scholta, J. Banhart, *J Power Sources*, 219 (2012) 120-125.
- [19] M.A. Hickner, N.P. Siegel, K.S. Chen, D.S. Hussey, D.L. Jacobson, M. Arif, *J Electrochem Soc*, 155 (2008) 427-434.
- [20] P. Boillat, G. Frei, E. H. Lehmann, G. G. Scherer, A. Wokaun, *Electrochemical and Solid-State Letters*, 13 (2010) 25-27.
- [21] R. Satija, D.L. Jacobson, M. Arif, S.A. Werner, *J Power Sources*, 129 (2004) 238-245.
- [22] M. Klages, S. Enz, H. Markötter, I. Manke, N. Kardjilov, J. Scholta, *J Power Sources*, 239 (2013) 596-603.

- [23] C. Tötzke, I. Manke, T. Arlt, H. Markötter, N. Kardjilov, A. Hilger, S.H. Williams, P. Krüger, R. Kuhn, C. Hartnig, J. Scholta, J. Banhart, Nucl. Instrum. Methods Phys. Res. Sect. A-Accel. Spectrom. Dect. Assoc. Equip., 663 (2012) 48-54.
- [24] M.A. Hickner, N.P. Siegel, K.S. Chen, D.N. McBrayer, D.S. Hussey, D.L. Jacobson, M. Arif, J Electrochem Soc, 153 (2006) A902-A908.
- [25] A. Lange, A. Kupsch, M.P. Hentschel, I. Manke, N. Kardjilov, T. Arlt, R. Grothausmann, J Power Sources, 196 (2011) 5293-5298.
- [26] D.S. Hussey, D.L. Jacobson, M. Arif, K.J. Coakley, D.F. Vecchia, J. Fuel Cell Sci. Technol., 7 (2010).
- [27] N. Kardjilov, A. Hilger, I. Manke, M. Strobl, M. Dawson, S. Williams, J. Banhart, Nuclear Instruments and Methods in Physics Research Section A: Accelerators, Spectrometers, Detectors and Associated Equipment, 651 (2011) 47-52.
- [28] S.H. Williams, A. Hilger, N. Kardjilov, I. Manke, M. Strobl, P.A. Douissard, T. Martin, H. Riesemeier, J. Banhart, J. Instrum., 7 (2012) 1-25.
- [29] N. Kardjilov, M. Dawson, A. Hilger, I. Manke, M. Strobl, D. Penumadu, F.H. Kim, F. Garcia-Moreno, J. Banhart, Nuclear Instruments and Methods in Physics Research Section A: Accelerators, Spectrometers, Detectors and Associated Equipment, 651 (2011) 95-99.
- [30] C. Tötzke, I. Manke, A. Hilger, G. Choinka, N. Kardjilov, T. Arlt, H. Markötter, A. Schröder, K. Wippermann, D. Stolten, C. Hartnig, P. Krüger, R. Kuhn, J. Banhart, J Power Sources, 196 (2011) 4631-4637.
- [31] J. Banhart, Advanced Tomographic Methods in Materials Research and Engineering, Oxford University Press, Oxford, UK 2008.
- [32] I. Manke, C. Hartnig, N. Kardjilov, M. Messerschmidt, A. Hilger, M. Strobl, W. Lehnert, J. Banhart, Appl Phys Lett, 92 (2008) 244101.
- [33] N. Kardjilov, I. Manke, A. Hilger, M. Strobl, J. Banhart, Materials Today, 14 (2011) 248-256.
- [34] M. Strobl, I. Manke, N. Kardjilov, A. Hilger, M. Dawson, J. Banhart, Journal of Physics D-Applied Physics, 42 (2009).
- [35] T. Arlt, M. Klages, M. Messerschmidt, H. Riesemeier, J. Scholta, J. Banhart, I. Manke, Ecs Electrochemistry Letters, 3 (2014) F7-F9.
- [36] P. Krüger, H. Markötter, J. Hausmann, M. Klages, T. Arlt, J. Banhart, C. Hartnig, I. Manke, J. Scholta, Journal of PowerSources, 196 (2011) 5250-5255.
- [37] H. Markötter, T. Arlt, J. Banhart, I. Manke, H. Riesemeier, P. Krüger, J. Haußmann, M. Klages, J. Scholta, Mater. Test., 55 (2013) 355-360.